Title: Mesoporous chitosan based conformable and resorbable biostrip for Dopamine detection

Md Abdul Kafi[1,2*], Ambarish Paul[2*], Anastasios Vilouras[2] and Ravinder Dahiya[2]

[1]Department of Microbiology and Hygiene, Bangladesh Agricultural University, Mymensingh 2202, Bangladesh.

[2]BEST group, James Watt School of Engineering, University of Glasgow, G128QQ, UK
*Equal contributing authors

Corresponding author: Ravinder Dahiya (E-mail: Ravinder.Dahiya@glasgow.ac.uk)

Abstract: This work presents a chitosan based resorbable biostrip for label-free electrochemical detection of dopamine (DA).The biostrip consists of mesoporous-chitosan-graphene oxide (m-Chit-GO) composite-based sensing electrode and graphene-based interconnects. Obtained with particulate leaching, the m-chit-GO showed average pore size of 1μmwith slow (2h) curing process. The response of DA on m-Chit-GO was investigated and compared with their bulk counterpart to study the effect of mesoporosity on voltammogram output signals. The voltammetric investigations were performed with three-electrode set-up using m-Chit-GO electrode as working electrode whereas Ag/AgCl and Graphene were used as a reference and counter electrodes, respectively. The quantitative analysis of concentration-dependent voltammetric peak-current enhancement revealed significantly higher response for m-Chit-GO (10pM) as compared to their bulk state (100nM) on DA. The presented resorbable biostrip offers a limit of detection of 10pM and thereby shows great promise for detection of DA levels for early diagnosis of neurodegenerative diseases.

Keywords: Biostrip, Chitosan, Dopamine, Graphene oxide, Bioresorbable Electronics

1. Introduction

Health management of elderly patients suffering from neurodegenerative (ND) diseases pose considerable challenge to healthcare sector and demands engineering solutions to forecast their incidence (Prince et al. 2016). The ND diseases, caused by impairment of dopaminergic activity of hippocampal neuron in the mid brain, give rise to memory-loss leading to worse impact on their quality life particularly when left unattended for longer period (Nobili et al. 2017). Early detection of dopamine (DA) impairment in patients could act as a forecast for remedial measures involving assistance from clinical experts at the early stage and thus demands highly sensitive platform that can selectively detect with a low limit of detection (LOD) (Thakur et al. 2018; Suominen et al. 2013).

Various types of currently practiced DA detection assays (Table-1) failed to achieve the desired LOD in the order of pM concentration necessary for its detection in body fluid. Although there are few devices offer reasonable sensitivity and low LOD, they involve bio-incompatible and non-degradable materials, which restrict their use in implantable electronics (Joshi et al. 2018; Lee et al. 2015). In addition, those devices often require surgery for their removal after use since they consist metallic substances as electrodes (Canevari et al. 2016; Cruz Moraes et al. 2008; Li et al. 2016; Nagles et al. 2017; Wang et al. 2017). For these reasons, the implantable devices with biodegradable and biocompatible constituents are in high demand for avoiding such complicated surgical procedures after use (Dahiya 2015; Muzzarelli et al. 2014). Considering those properties together with sensing property and compatibility with microfabrication process, chitosan has attracted much attention for wearable and implantable applications (Kafi et al. 2017, Kafi et al. 2018, Kafi et al. 2019). This biopolymer has spurious supply of amino and hydroxyl groups offering ready chemical reaction with cross-linkers and bio-analytes and thus was selected for this biostrip fabrication (Mitra et al. 2013). In this work, we used graphene oxide as crosslinker of chitosan molecules passivating it from hydrolysis under electrochemical investigation. Previously we have demonstrated Chitosan graphene

oxide (Chit-GO) composite as bio-electrode with graphite paper as interconnect as DA detection (Kafi et al. 2017; Kafi et al. 2011).

Table 1: Comparison of analytic performance and compatibility of proposed bio-strip with previously reported DA sensor

Material	Detection Method	LOD µM	Linear response µM	Green technology compliance	Ref
GCE/SWNT/ CoPC	CV, DPV	0.2	3.11-93.2	no	Moraes et al. 2008
GCE/NC-QD	DPV	0.005	0.05-2	no	Canevaria et al. 2016
GCE/Pb/RGO	CV, DPV	0.18	0.45-421	no	Wang et al. 2017
GCE/NeO/Chit	CV, DPV	0.079	0.09-16		Nagles et al. 2017
GCE/RGO/Pd	CV	0.03	0.1-2.63	no	Li et al. 2016
Chit-GO bio-strip	electrochemical	0.00001	0.00001 -100	yes	This work

GCE/SWNT/CoPC: Glassy carbon electrode modified single walled carbon nanotube and cobalt. GCE/NC-OD: GCE modified monocrystalline carbon quantum dot. GCE/Pb/RGO: GCE modified cubic Pb and reduced graphene oxide. GCE/NeO/Chit: GCE modified Neodymium(III) oxide and

In this work, we have successfully fabricated bendable biostrip with mesoporous-Chit GO (m-Chit-GO) composite-working electrodes (WE) for label free electrochemical detection of DA, as illustrated in Figure 1. The use of m-Chit-GO electrode drastically lowers the limit of detection LOD to 10pM which allowed the as fabricated bio-strip suitable for in vivo DA detection. The device is wholly biodegradable and bioresorbable since it employs eco-friendly materials like Chitosan, GO and graphene (Grande et al. 2017; Zuo et al. 2013). Since the device was fabricated on a flexible chitosan membrane it is conformable on curvy surfaces of organs and tissues. The m-Chit GO based biostrip offers low LOD = 10pM and good stability required for continuous trace detection of DA in early-stage impairment of dopaminergic neurons, commonly found in the elderly population. The biostrip provides high selectivity to DA detection against interfering agents like ascorbic acid (AA) and uric acid (UA), which coexist in the body fluid (Nobili et al. 2017). The biostrip can be integrated with a miniaturized low-power application specific integrated circuit (ASIC), powered by a wireless charging coil, for

for data transmission. The fabricated 3-electrode sensor could be interfaced with the "positive feedback" potentiostat circuit to compensate for any Ohmic-drop across the Counter (CE) and the Working Electrode (WE) by automatically adjusting the value of $R_{VARIABLE}$ to generate a wave that can be added to the input voltage, as shown in Supplementary Figure 3. Since the device involves biocompatible materials and utilizes eco-friendly fabrication process, the work aligns well with green technology.

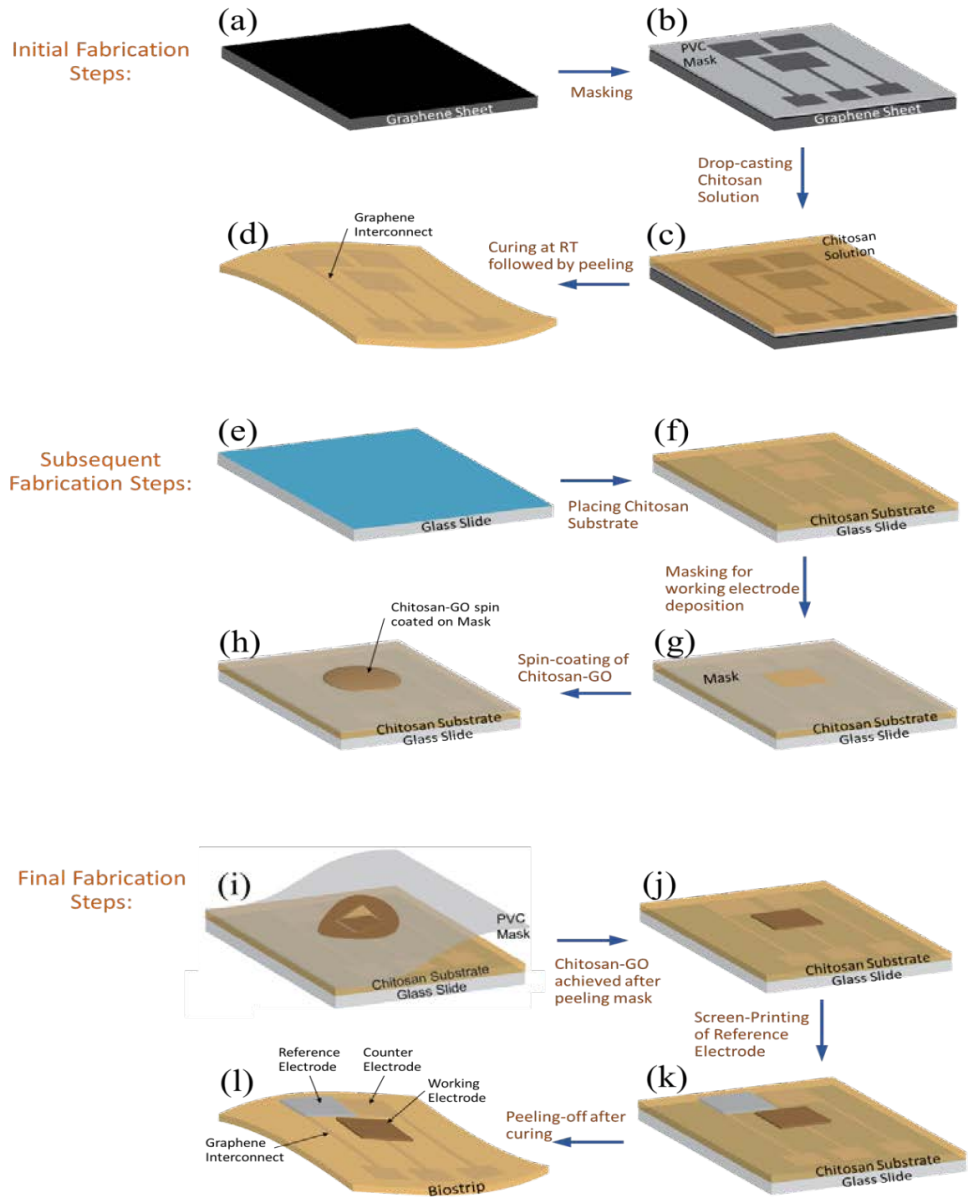

Figure 1. Schematic representations of the fabrication process flow. Initial fabrication step: Cast printed graphene interconnect on chitosan substrate, which includes placement of mask on the graphene sheet, drop-casting of chitosan solution on the mask and Peeling

off chitosan substrate after curing. Subsequent fabrication step: spin coating of Chit-GO sensor that includes placing of chitosan substrate on glass slide, masking over the chitosan substrate leaving opening for working electrode establishment and spin coating of Chitosan-GO for establishing working electrode. Final fabrication step: preparation of Chitosan-GO bio-strip, which includes peeling of mask (followed by leaching process to achieve porous device) mask removal, screen printing of Ag/AgCl reference electrode and peeling of the bio-strip.

2. Material and methods

2.1 Materials and reagents: Chitosan powder and Phosphate buffered saline (PBS) (pH 7.4, 10mM) were obtained from Sigma-Aldrich Spruce, USA. Graphene Oxide (GO) was obtained from Graphene Laboratories Inc. NY, USA. D-(+)-Glucose, AA and UA were obtained from Sigma, Life science. Dopamine (DA) hydrochloride powder was purchased from Alfa Aesar, Thermos Fisher Scientific. Millipore Deionized (DI) with resistivity 18MΩ-cm was water used in the experiments. All the chemicals were analytical grade reagents.

2.2. Biostrip design and fabrication: The chitosan based biostrip with patterned graphene layers as interconnects was designed to achieve three-electrode configuration for electrochemical measurements and DA sensor development. The fabrication of the biostrip was achieved by drop-casting of chitosan solution through PVC hard mask followed by cast printing of graphene flakes network interconnects as shown in Figure 1.

2.2.1 Design of biostrip: The biostrip on chitosan substrate with patterned graphene layers as interconnects was designed to have three-electrode configuration (Fig. 2) for electrochemical measurements and DA sensor development. The three-electrode set-up consists of working electrode (WE), reference electrode (RE) and counter electrode (CE) which are connected to respective pads for electrical connections with a Potentiostat. The dimensions of WE, are 3×3mm, and that of the RE and CE are 3×2.5mm each. The graphene interconnects with width

1.5 mm connects the electrodes with the contact pads. The dimension of designed bio-strip is $3\times1.5cm^2$.

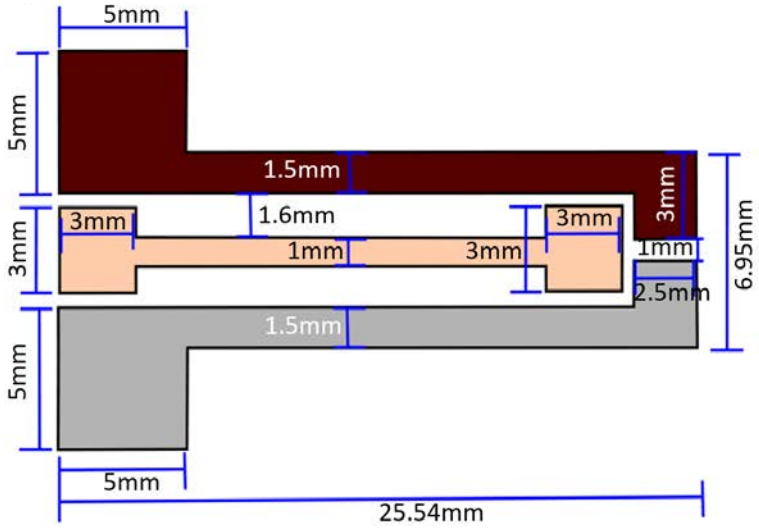

Figure 2. Design of Bio-strip showing the working electrode (WE), reference electrode (RE) and counter electrode (CE) connected to their respective contact pads through interconnects.

2.2.2 Device fabrication: The device fabrication involves mask-assisted cast printing of graphene patterns on chitosan substrate, development of m-Chit-GO W.E. which forms the active sensing material, and establishment of the Ag/AgCl-based RE. Graphene is employed as interconnects as well as the CE. The fabrication steps of the bio-strip are described below-

Preparation of Chitosan substrate: Chitosan membrane of high MW was used as a substrate for the fabrication of the biostrip bearing GO-Chit WE and Ag/AgCl RE while unmodified transferred graphene layer was used as the CE. High MW chitosan was used as the substrate because of its high mechanical stability due to the long polymeric chain. To prepare 1% chitosan solution, 500mg of chitosan powder was added to 44.6ml of DI water and stirred in a magnetic stirrer at 1200rpm for 1hr at 37^0C to achieve uniform dispersion. The chitosan is acetylated by the addition of 4.4ml of acetic acid to form a thick jelly like solution. The acetylated chitosan solution was aspirated and stored at 4^0C for solution casting as described below.

Cast printing of graphene on chitosan membrane for interconnects: The graphene interconnects of the bio-strip were fabricated using solution assisted cast-printing of graphene layers on chitosan substrate. This was achieved by drop-casting chitosan solution on graphene sheet through PVC hard mask as shown in Figure-1. The design for PVC hard mask was obtained in L-edit and realized through a blade-cutter (Silhouette Cameo 2). The chitosan membrane formed on the hard-masked graphene sheet was dried at RT for 12h before peeling off. Continuous and uniform layers of mechanically exfoliated crumpled graphene flakes were transferred to the chitosan substrate in the region where the chitosan solution was exposed to graphene sheet. The chitosan membrane with graphene interconnects was peeled off and fixed on a rigid glass substrate for deposition of Chit-GO WE and Ag/AgCl RE.

Preparation and deposition of mesoporous Chit-GO WE: The m-Chit-GO electrode was prepared by particulate leaching process where Glucose granules of average particle size 5µm were used as the particulate and Chit-GO as the matrix. During the slow curing process (2h) the sugar particle was leached and became of size around 1µm prior solidification and thus gave pore sizes of around 1µm. Chit-GO solution was prepared by using the same procedure as described above for the preparation of the Chitosan solution. However, in the preparation of Chit-GO solution, 2ml of as received GO aqueous solution was added to 50ml of DI water prior to the addition of Chitosan. The Chit-GO solution contains a uniform dispersion of GO micro-sheets and forms a GO network throughout the bulk of Chit-GO solution. Granulated glucose of average size 5µm was grinded in a mortar and pestle to yield a uniform size distribution before mixing with as prepared Chit-GO solution in the ratio 5:3 by wt. The resultant mixture was cast on the PVC hard mask and spun at different spinning speeds of 200, 400, 600 and 800rpm for 2min to yield uniform deposition of Chit-GO membrane as shown in supplementary Figure 1. The sample was immersed in DI water to dissolve the Glucose granules resulting in the formation of m-Chit-GO as shown in supplementary Figure 2. The m-Chit-GO WE realized

when the PVC hard mask was peeled off from the substrate. The morphology of the m-Chit-GO electrodes was investigated with a scanning electron microscope (SEM). The non-porous Chit-GO WE was fabricated by an identical spinning process using Chit-GO solution without glucose granules.

Deposition of Ag/AgCl RE: The Ag/AgCl RE was screen-printed through a hard mask as shown in Figure 2. Finally, the Chitosan-based biostrip was removed from the glass substrate and subsequent the electrochemical characterization was performed as described below.**2.3 Morphological and Electrochemical investigations:** The FESEM images were obtained using, Hitachi S-4700, at an accelerated voltage of 10KV and 10mA current. The optical micrographs were obtained from Nikon Eclipse LV100ND microscope connected with Leica MC170HD camera. FTIR investigation was performed using VERTEX 70, BRUKER spectrometer.

The SEM images acquired for morphological investigations are shown in the Figure 3 d-f and Supplementary Section S1. Cyclic voltammetry (CV) and linear sweep voltammetry (LSV) were employed for electrochemical detection of DA using a standard electrochemical workstation with PGSTAT 302N (Metrohm Auto lab) controlled by "Autolab software". A three-electrode setup was applied using the fabricated biostrip as WE, where Ag/AgCl and Graphene served as RE and CE, respectively. PBS was used as electrolyte throughout the experiments. All experiments were repeated thrice with freshly prepared devices providing an identical condition for obtaining the statistical errors.

3. Results and discussions

The porous (m-Chit-GO) and non-porous (bulk Chit-GO) chitosan-based disposable biostrips were fabricated and electrochemically evaluated under identical conditions to study the effect of porous morphology on sensing performances. The fabrication steps were confirmed by both

optical and SEM analysis. The optical images presented in Figure 3a-c demonstrate the formation of the chitosan-based biostrips, where transferred graphene and spin-coated Chit-GO are shown sequentially during the device fabrication. The porous morphology of m-Chit-GO, obtained via particulate leaching, was further confirmed using FESEM. The SEM images obtained from each fabrication step are illustrated in Figure 3d-f, where Figure 1d demonstrates a thin layer of graphene transferred on the chitosan substrate, and Figure 3e and 3f reveal distinct topographic variations from bulk Chit-GO and its porous counterpart. The pore dimensions of the Chit-GO device showed dependence on spinning speeds and glucose particle size during fabrication (Supplementary Fig. 1 and 2).

The FTIR analysis of GO shows the existence of C=O in carboxylic group at 1721 cm^{-1}, C=C in conjugated ketones at 1620 cm^{-1}, phenol C-O stretch at 1200 cm^{-1} and primary alcohol C-O stretch at 1030 cm^{-1} (Fig. 3g). The chitosan absorbance peak at 1547 cm^{-1} is attributed to the secondary amide –N-H bending. The $–NH_2$ group of chitosan reacts with the –C=O group of GO to form an amide (-NHC=O) linkage between the two molecules (Bustos-Ramírez et al. 2013; Zuo et al. 2013). The formation of an amide linkage is confirmed by (a) the shift in the –NH bending peak of chitosan towards the lower wave number side to 1549 cm^{-1} in GO chitosan, (b) disappearance of the –C=O peak obtained for GO in the GO chitosan sample, and (c) higher intensity of –CO stretching vibration peak at 1060 cm^{-1} as compared to the same in GO at 1030 cm^{-1} (Emadi et al. 2017). The occurrence of amide linkage in Chit-GO prevents the ready dissolution of the composite in an aqueous medium.

The biodegradability of the biostrip in aqueous medium was investigated by determining the swelling ratio of equal weighed samples of the bulk and m-Chit GO electrodes when exposed to water (Pabari and Ramtoola 2012). The swelling ratio of both porous and nonporous bulk Chit-GO increased significantly in the first 24h of aqueous exposure. Beyond this time the rate of water absorption decreased and led to disintegration of the electrodes. The maximum swelling ratio attained by the bulk and m-Chit GO electrodes was found to be 80% and 110%

respectively before disintegration (Fig. 3h). After this, the porous device was evaluated for signal stability. The device showed good electrical continuity for the first 56 cycles, beyond which the degradation started as shown in Figure 3i. The peak current of 0.425V decreases monotonically for the first 45 cycles after which the current stabilizes (Fig. 3i inset). Thus, all electrochemical measurements were performed by pre-exposing the samples through the same cycles of operations for the consistent and stable output signal.

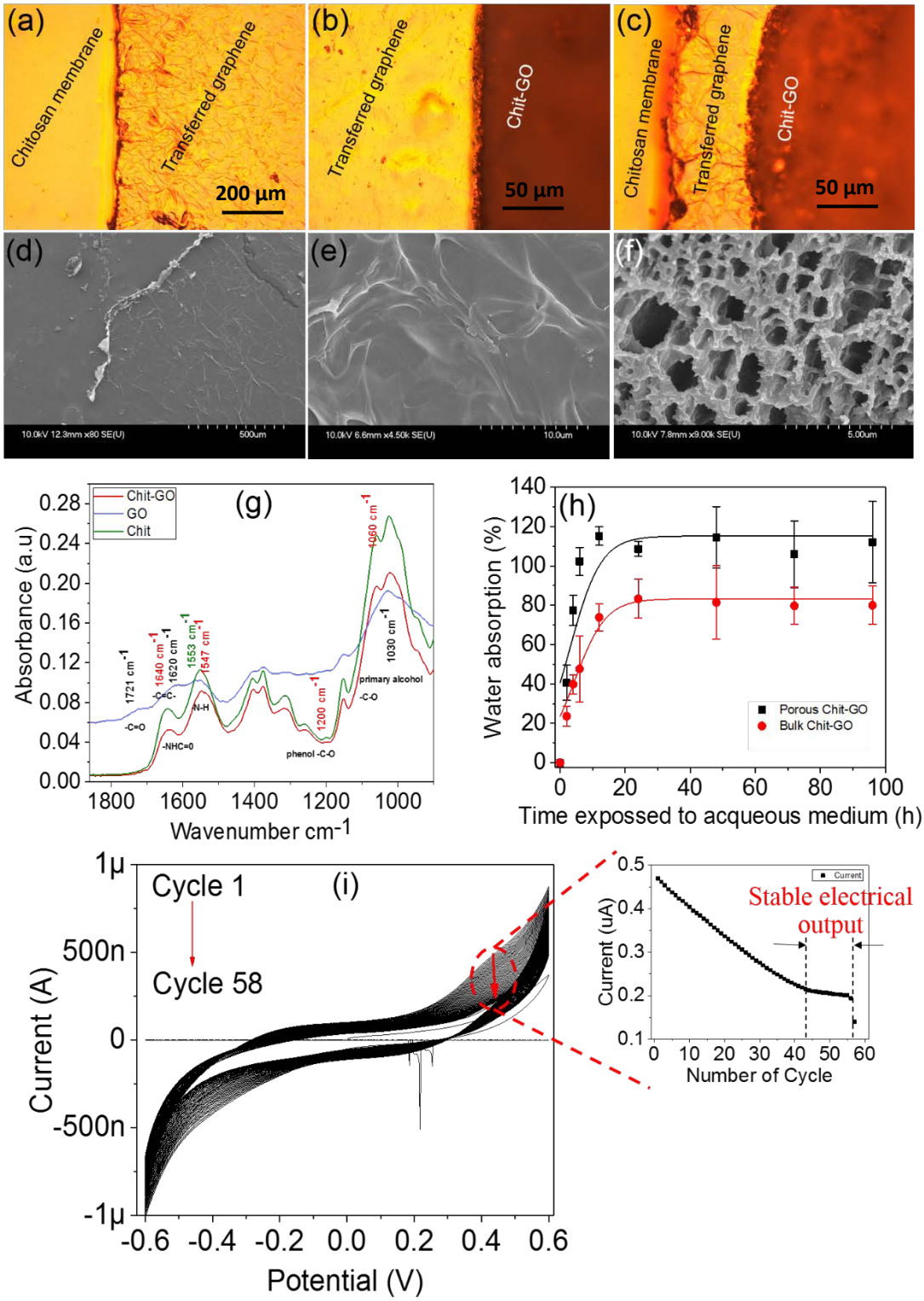

Figure 3. Microscopic image of (a) castprinted graphene network on chitosan substrate, (b) deposited m-Chit-GO layer on castprinted graphene network and (c) m-Chit-GO WE on graphene network interconnect of the biostrip (ref. Fig. 1. For detailed fabrication process). FESEM images of (d) castprinted graphene network as interconnect, (e) bulk Chit-GO WE and

(f) mesoporous (m)-Chit-GO WE, (g) FTIR spectrographs of pristine Chitosan, GO and Chitosan-GO composite in the range of 2000 cm^{-1} to 900 cm^{-1}. (h) Plot of swelling ratio vs. time for bulk and m-Chit GO electrodes showing the increased stability of the later in aquoues medium and (i) Repeatative CV investigation for 57 cycles with m-Chit GO electrodes in PBS (pH 7.4) (inset: Peak currentobtained at 0.4 V vs. number of cycles plots howing the termination of electrical connections at 57 cycles due to swelling).

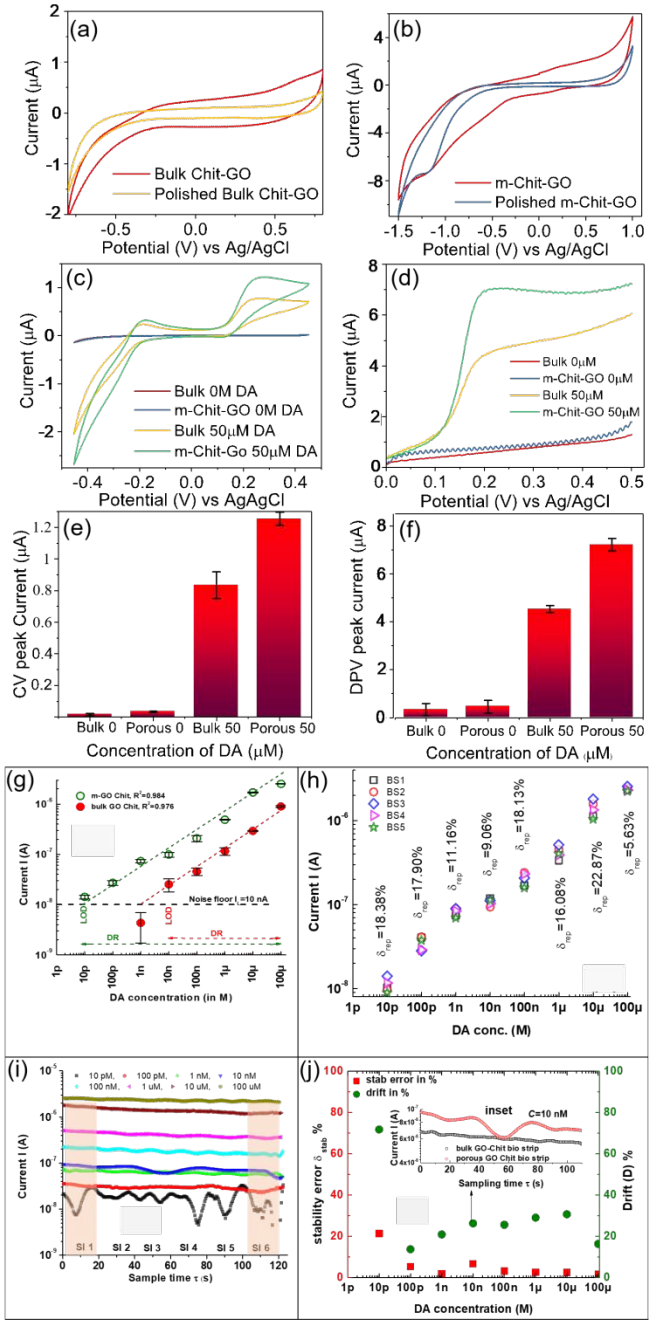

Figure 4. Characterization of Chit-GO biostrips: CV ofbulkChit-GO (a) and mesoporousChit-GO (b) beforeand after electropolishing. CV (c) and LSV (d) of DA measured with the polished mesoporous Chit-GO electrode and the current peaks obtained from CV (e) and linear swipe voltammetry (f) are shown. Data are the mean ± standard deviation obtained from identically performed three experiments. Current I vs. DA concentration. Calibration plot for (g) bulk and m-Chit-GO based bio-strip in the experimental range 10pM - 100μM and, (h) five identical samples of m-Chit-GO based bio-strip showing the reproducibility error for different DA concentrations in the experimental range, (i) Current I vs. time plotfor different DA concentrations recorded for a total sampling time τ=120 s showing the electrical stability and drift in sensor performance over time and (j) Stability errorδ_{stab} and drift D% vs DA concentration plotfor m-Chit-GO based bio-strip, (inset) Comparative current vs time plot for bulk and m-Chit-GO based biostrips for C= 10nM.

Three-electrode voltammetry (CV and linear sweep voltammetry (LSV)) was carried out for electrochemical characterization and sensing application. The CV from the bulk Chit-GO device showed background current without any peak when scanned in PBS at a scan rate of 15mV/s (Fig. 4a). Then the device was electro-polished applying 50 scan cycles to minimize such background current (Kafi et al. 2011; Kafi et al. 2010). Likewise, background current with higher intensity, observed from the mesoporous electrode, were also electro-polished with a wider potential window of -1.5 to 1.0V while a reduction peak between -1.1 and -1.2V was noticed unlike the bulk (Fig. 4b). This peak could be due to the reduction of air (O_2) trapped within the pores of the device (Kafi et al. 2010). Such background was sufficiently minimized at the desired operating windows of -0.5 to 0.5V (Fig. 4b) as most of the catecholamine's redox has been reported in that potential (Peltola et al. 2017; Zhou et al. 2013).Therefore, this potential window was employed for the electrochemical investigations throughout this research.

Cyclic Voltamogram from bulk and m-Chit-GO working electrodes in 50µM DA showed characteristic quasi-reversible redox phenomenon, with current peaks at -0.275V and 0.225V, with varying intensities whereas such redox phenomenon was absent when fresh PBS employed showed in Figure 4c. However, enhancement in cathodic peak intensity was greater than anodic peak for both sensor types and thus variation was also observed with LSV in 50µM DA with 0 to 0.5V at a scan 0.15V/s (Fig. 4d). The results revealed a current peak at 0.2V with varying intensities- both methods indicating similar peak enhancement in the case of the m-Chit-GO electrode (Fig. 4e-f). As a biomaterial-based sensor, the sensitivity of chitosan biostrip is influenced by the scanning period. Thus, even though both analytic methods employed similar principle, their sensitivity varied because of the variation of scanning period. The CV scanning of a wider potential window of -0.5V to 0.5V at a scan rate of 15mV/s required 66.67 second while LSV scanning of 0.0 to 0.5V at a similar scan rate required 6.67 second. This variation in scanning period was responsible for such difference in peak current. It has been reported that repeated anodic and cathodic redox resulted in the accumulation redox couples on the electrode surface that have impacted on in the intensities of peak currents (Bery and Grivell,1995; Kafi et al. 2010; Kafi et al 2011). Thus between these two voltammetry methods, the highest enhancement in the current peak was observed from LSV, which is obvious due to the rapid, fast and sensitive detection nature of LSV (Bartlett 2008). Hence, LSV peak was considered a sensitive parameter for all electrochemical investigations in this research.

The sensor performance was investigated with anodic current (I) obtained from both the bulk and m-Chit-GO-based bio-strips, exposed to different DA concentrations in the range of 10pM-100µM (Fig. 4g-j). The CV anodic peak for both the bulk and the porous Chit-GO based bio-strips occurs in the neighborhood of 0.2V (Fig. 4 c-d), when the applied potential window is -0.5V to 0.5V, and therefore the bio-strip was characterized at a constant operating voltage of 0.2 V. The static measurements for current (I), for both bulk and porous counterparts, were repeated three times for each DA concentration. For each DA concentration, the deviations in

anodic current (ΔI) from the mean (I) were calculated over the statistical sample size and are represented as error bars in Figure 4g. The mean I for each data set, for both bulk and porous counterparts, were calculated for different DA concentrations and plotted in the logarithmic scale. In the logarithmic scale, the anodic current (I) showed a linear relation with DA concentration (C) and obeyed the following equations for bulk and m-Chit-GO-based bio-strips, respectively:

$$\log I = (0.361 \pm 0.023) \log C - (4.54 \pm 0.143) \quad (1)$$

$$\log I = (0.327 \pm 0.015) \log C - (4.281 \pm 0.121) \quad (2)$$

Output signal below I_L=10nA is associated with low signal to noise ratio due to experimental constraints and was thus in appropriate for experimental analysis. Thus, I_L=10nA is referred to as the noise floor in this work. The lower detection limit (LOD) is defined as the lowest DA concentration that can be measured using the bio-strip. It was graphically obtained by extrapolating the calibration curve to intercept the I_L=10nA at the specified concentration of DA, below which the instrument failed to detect. Although the LOD for the bulk Chit-GO bio-strip was graphically found to be 1nM using Figure 4g, the measurement suffered from low signal to noise ratio S/N<3. The LOD of the bulk Chit-GO and m-Chit GO based bio-strip was graphically determined to be 10nM and 10pM respectively as depicted in Figure 4g. The three-order of reduction in the LOD of m-Chit-GO bio-strip, as compared to its bulk counterpart, could be attributed to the high surface area of the mesoporous morphology of the working electrode. This contributed to the increased redox reaction sites for the DA molecules. However, the sensitivities S of both biostrips, as calculated from the slope of the calibration curve in Figure 4g, revealed that there is no significant enhancement in the performance of m-Chit-GO biostrip based sensors when compared with its bulk counterpart. Reduced LOD of the as-fabricated m-Chit-GO bio-strip is most suitable in applications where the trace detection of DA is required with good sensitivity. To ascertain the reproducibility of the fabrication process, experiments were repeated with five identical m-Chit-GO biostrips for all DA concentrations

and under identical ambient conditions, as shown in Figure 4h. The reproducibility error δ_{rep} of the as-fabricated bio-strip was calculated using $\delta_{rep} = (\Delta I/I_{mean})$ x100, where ΔI and I_{mean} are the standard deviation in (I) and the mean (I) respectively. The δ_{rep} was found to vary between 5.06-22.87%in the whole experimental range. The low δ_{rep} of the bio-strip makes them suitable for continuous monitoring of trace concentrations of DA at synaptic junctions of the neurons in the brain.

Chemical sensors often suffer from inconsistency and drift in electrical signals when operated over a long duration of time. This electrical instability in data acquisition restricts the use of devices for application requiring continuous monitoring. Thus, electrical stability of the current (I) in as fabricated m-Chit-GO-based bio-strip was investigated in terms of short-time stability δ_{stab} and longtime stability in the form of drift D. These measurements were performed using chrono-amperometric method by exposing the bio-strip to different DA concentrations. The measurements were performed at ambient temperature and pressure and at an applied bias voltage of 0.2 V. All measurements were performed over a total sampling time τ = 120 s, with a sampling interval of 0.5s for each DA concentration in the experimental range, as shown in Figure 4i. The stability error δ_{stab} is calculated using $\delta_{stab} = (\Delta I/I_{mean})$x100, where ΔI represents the standard deviation in (I) for the chosen sample size over τ and I_{mean} represents the mean (I) over that interval. Since the data recorded from the bio-strip contains electronic noise along with chemical drift when operated over an extended duration of time, the data was statistically analyzed over both short and long-time duration. To ascertain the influence of electronic noise on the performance of the biostrip sensor, the total sampling time was divided into six equal sample intervals (SI) of 20s durations and δ_{stab} was calculated for each interval using above expression. The δ_{stab} of the biostrip, obtained from the mean δ_{stab} over all sample intervals is plotted in Figure 4j. The δ_{stab} in the concentration range of 100pM to 100 μM was found to be between 2.1 - 5.3% and this increased to 21.35% for C=10pM. As the DA molecules at C=10pM were highly reduced in number, their availability to produce redox reactions at the WE surface

was low and unsteady over time and this led to unstable electrical signal and high δ_{stab}. Taking into consideration the fact that biodegradability of the biostrips may influence the steady electrical output, the δ_{stab} was also obtained in the C range of 100pM to 100µM and it was found to be low. This means the biostrips hold promise for continuous measurements.

The drift in the output of chemical sensors is another issue and m-Chit GO biostrips were also assessed for the same. The results in Figure 4i and 4j show the drift in current (I) for all DA concentrations during an extended sampling time of 120s. The drifts in sensor performance over different DA concentration were measured in terms of normalized variation of the mean current obtained from the first (SI1) and sixth SI(SI6) as depicted by the equation:

$$D\% = [\{I_{(mean)SI1} - I_{(mean)SI6}\} / I_{(mean)SI1}] x\ 100 \qquad (3)$$

Where $I_{(mean)SI1}$ and $I_{(mean)si6}$ represent the mean (I) of the SI1 and SI6 respectively. The percentage drift (D%) in (I), calculated using Eq (3), is as shown in Figure 4j. In the concentration range of 100pM-100µM, the drift was found to be between 13.7 - 30.7%. It was found to be high for C=10pM. The drift in I, for the bulk Chit-GO based biostrip for C=10nM was found to be 17% (Figure 4j (inset)). This is within the D% range obtained for the porous counterpart. High drift in the signal current of the m-Chit GO bio-strip, especially for C=10pM, could be attributed to the exhaustion of the DA molecules with time due to the redox reaction occurring at the surface of the m-Chit GO electrode. The reduction in drift for increased concentrations of DA could be attributed to the decrease in the signal current I due to the passivation of the WE surface with redox products on prolonged exposure. Thus, the m-Chit-GO-based biostrip offers a wide dynamic range of 10pM-100µM, good stability in the electrical output and reduced drift. Owing to its biodegradability, high electrical stability and capability for detecting trace concentrations of DA in the order of tens of pM, them-Chit-GO biostrip offers an attractive solution for continuous monitoring of DA in the synaptic junctions of the nerve cells.

The specificity of the m-Chit-GO biostrip for DA was also investigated using CV with uric acid (UA) and ascorbic acid as (AA) as interfering agents with C=50μM of the analytes.The stoichiometric differences of the analytes DA, AA and UA is evident from the CV investigation as shown in Figure 5a (Gualandi et al. 2018). Two separate redox peaks from DA and UA were observed at 0.2V and 0.4V, respectively, whereas a wide peak between 0.2 to 0.4V was observed from AA indicating the redox peaks are analyte specific. When DA redox peaks were compared with that from a mixture of DA and UA solutions (Fig. 5b), later revealed two distinctly separated anodic peaks of significantly enhanced current intensity (Atyah et al. 2017) and was attributed to the increased concentration of DA-UA solution (Nayak et al. 2016). This was confirmed by the disappearance of AA peaks when similar experiments were conducted with DA and AA mixture solutions (Fig. 5c).

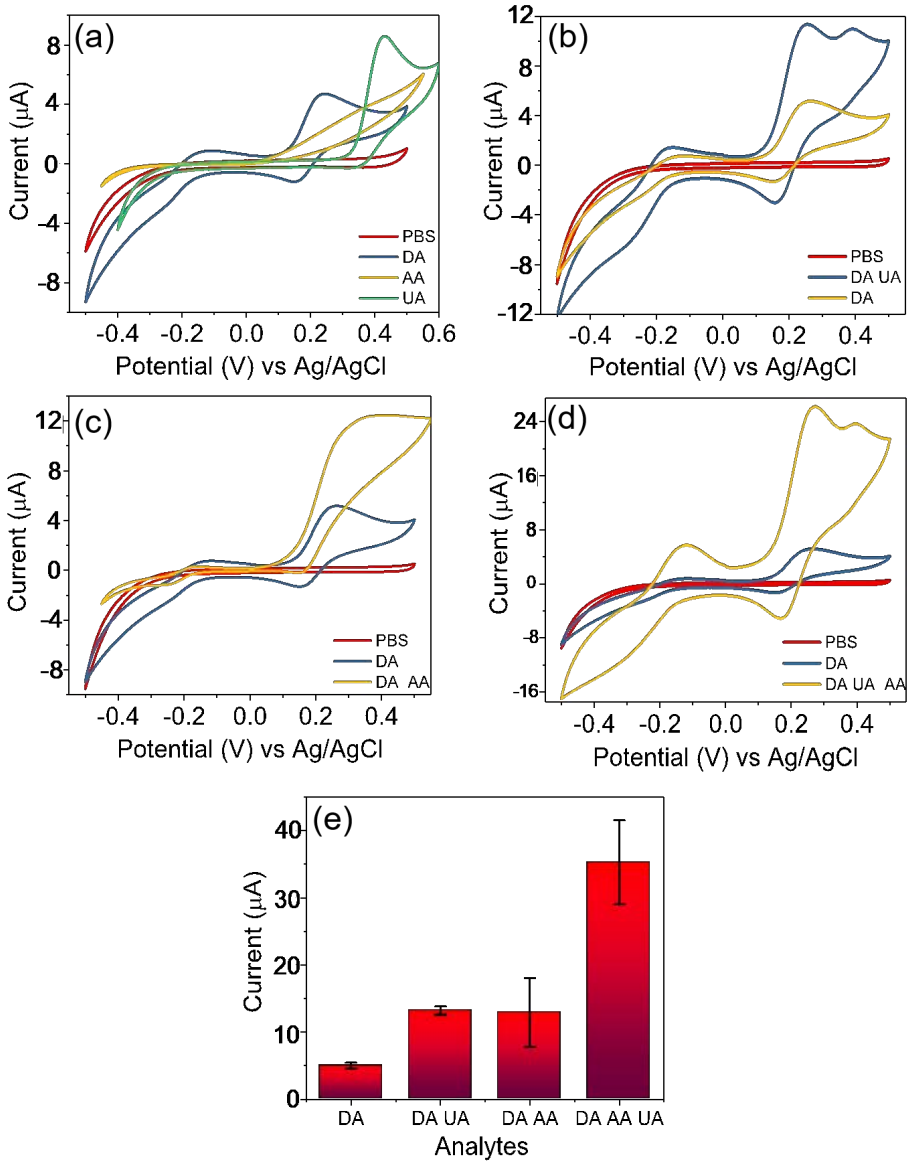

Figure 5. The specificity of m-Chit GO biostrip for Dopamine (DA): CV investigations of (a) separate solutions of analytes DA, AA and UA at C=50 μM, (b) DA-UA mixture, (c) DA-AA mixture and (d) DA-UA-AA mixture, and compared with equal C of DA. (e) Histogram representation for comparative analysis of CV peak intensities of DA-UA, DA-AA and DA-UA-AA mixtures with that of DA solution. Standard deviation about mean was obtained from three experiments with identically separate samples.

This is obvious because AA provides a peak over a wide area between 0.2V to 0.4V, instead of a single peak. When the experiment was repeated with a mixture of DA, UA and AA, no

characteristics peak of AA can be resolved in the high intensity DA and UA characteristic peaks as shown in Figure 5d. However, the significant peak enhancement compared to dual combinations indicated its presence in the mixture (Fig. 5e). Thus, the current peak position for DA, measured at 0.2V in all occasions, indicated its presence is independent of any other coexisting analytes (Gualandi et al. 2018). The anodic peak intensity was observed to dominate over cathodic peak for all analytes investigated. Hence, the anodic peak is proposed as the analytic method of this DA sensor.

4. Conclusions

This work reports the development of bendable chitosan based biostrip with mesoporous Chitosan-Graphene-Oxide (m-Chit GO) working electrode (WE) and cast printed graphene network interconnects for label free trace detection of dopamine (DA). Electrochemical investigations on bulk and m-Chit GO WE based biostrips showed a significantly lower limit of detection (LOD). The reduction in LOD is attributed to the increased surface area of mesoporous electrodes which provided increased redox sites for DA molecules. Due to the drastic reduction in LOD the m-Chit-GO biostrips hold great promise for trace detection of DA, especially in the synaptic junctions of the brain. The biostrip offers excellent electrical stability with stability error of 5.3% and reduced drift in sensor output which makes it suitable for continuous monitoring. The biostrip shows good selectivity for DA redox peaks against interfering signals of UAand AA redox peaks in the same potential window. However, at low concentrations, an increased drift is observed in the output of the biostrip and they must be calibrated before use. Based on bioresorbable materials and fabricated with an eco-friendly process, the ultra-thin flexible biostrips presented here are most suited for implantable applications where conformability on soft and curvy tissues is an important requirement.

Conflicts of interest

There are no conflicts to declare

Acknowledgements

This work was supported in part by the European Commission through Marie Curie Fellowship (H2020-MSCA-IF-2015-704807), the Academy of Medical Sciences (NF161567) and EPSRC through Engineering Fellowship for Growth - (EP/M002527/1 and EP/R029644/1).

References

Atyah, M.B., Bounab, L., Choukairi, M., El Khamlichi, R., Bouchta, D., Chaouket, F., Raissouni, I., 2017. J. Mater. Environ. Sci. DOI:10.26872/jmes.2018.9.1.8
Bartlett, P.N., 2008. Bioelectrochemistry: fundamentals, experimental techniques and applications. John Wiley & Sons.
Bery, M.N., Grivell, M.B., 1995. In: Walz, D., Berry, H., Milazzo, G. (Eds.), Bio-electrochemistry of Cells and Tissues. Verlag, Birkhauser, Basel, pp. 134–158
Bhagat, V., Becker, M.L., 2017. Biomacromol. 18(10), 3009-3039.
Bustos-Ramírez, K., Martínez-Hernández, A., Martínez-Barrera, G., Icaza, M., Castaño, V., Velasco-Santos, C., 2013. Materials 6(3), 911-926.
Canevari, T.C., Nakamura, M., Cincotto, F.H., de Melo, F.M., Toma, H.E., 2016. Electrochim. Acta 209, 464-470.
Cruz Moraes, F., Cabral, M.F., Machado, S.A., Mascaro, L.H., 2008. 20(8), 851-857.
Dahiya, R.S., 2015. Epidermial electronics: flexible electronics for biomedical applications. Handbook of Bioelectronics: Directly Interfacing Electronics and Biological Systems. Cambridge University Press: Cambridge, pp. 245-255.
Dang, W., Manjakkal, L., Navaraj, W.T., Lorenzelli, L., Vinciguerra, V., Dahiya, R., 2018. Biosens. Bioelectron. 107, 192-202.
de Queiroz Antonino, R., Lia Fook, B., de Oliveira Lima, V., de Farias Rached, R., Lima, E., da Silva Lima, R., Peniche Covas, C., Lia Fook, M., 2017. Mar. Drugs 15(5), 141.
Emadi, F., Amini, A., Gholami, A., Ghasemi, Y., 2017. Sci. Rep. 7, 42258.
Grande, C.D., Mangadlao, J., Fan, J., De Leon, A., Delgado-Ospina, J., Rojas, J.G., Rodrigues, D.F., Advincula, R., 2017. Macromol. Symp., p. 1600114. Wiley Online Library.
Gualandi, I., Tessarolo, M., Mariani, F., Cramer, T., Tonelli, D., Scavetta, E., Fraboni, B., 2018. Sens. Actu. B: Chemical 273, 834-841.
Honarkar, H., Barikani, M., 2009. Hengameh Chem. 140(12), 1403.
Jantsch, A., Anzanpour, A., Kholerdi, H., Azimi, I., Siafara, L.C., Rahmani, A.M., TaheriNejad, N., Liljeberg, P., Dutt, N., 2018. 19th IEEE International Symposium, pp. 370-375.
Joshi, S., Bhatt, V., Märtl, A., Becherer, M., Lugli, P., 2018. Biosensors 8(1), 9.
Kafi, M.A., Kim, T.-H., An, J.H., Choi, J.-W., 2011. Anal. Chem. 83(6), 2104-2111.
Kafi, M.A., Kim, T.-H., Yea, C.-H., Kim, H., Choi, J.-W., 2010. Biosens. Bioelectron. 26(4), 1359-1365.
Kafi, M.A., Paul, A., Dahiya, R., 2017. IEEE Sens. Conf. Glasgow, UK, pp. 1-4.
Kafi, M.A., Paul, A., A. Vilouras, R. Dahiya, 2018. IEEE Sens. Conf., N. Delhi, India,pp. 1-4.
Md. A. Kafi, Mst. K. Aktar, M. Todo, R. Dahiya. 2019. Regenerative Biomaterials, rbz034, (DOI: 10.1093/rb/rbz034)
Kafi, M.A., Paul, A., Vilouras,A., Hosseini, E. S., Dahiya, R. 2019. IEEE Sensors Journal (DOI - 10.1109/JSEN.2019.2928807).
Lee, J.S., Oh, J., Kim, S.G., Jang, J., 2015. Small 11(20), 2399-2406.

Li, D.-W., Luo, L., Lv, P.-F., Wang, Q.-Q., Lu, K.-Y., Wei, A.-F., Wei, Q.-F., 2016. Bioinorg. Chem. Appl. 2016.
Mitra, T., Sailakshmi, G., Gnanamani, A., Mandal, A., 2013. Mat. Res. 16(4), 755-765.
Moraes, F. C., Cabral, M. F., Machado, S. A. S., Mascaroa, L. H. 2008, *Electroanalysis.* 20, 851.
Muzzarelli, R., Mehtedi, M., Mattioli-Belmonte, M., 2014. Mar. Drugs 12(11), 5468-5502.
Nagles, E., Calderón, J.A., García-Beltrán, O., 2017. Electroanal. 29(4), 1081-1087.
Nayak, P., Kurra, N., Xia, C., Alshareef, H.N., 2016. Adv. Electron. Mater. 2(10), 1600185.
Nobili, A., Latagliata, E.C., Viscomi, M.T., Cavallucci, V., Cutuli, D., Giacovazzo, G., Krashia, P., Rizzo, F.R., Marino, R., Federici, M., 2017. Nat. Commun. 8, 14727.
Nyein, H.Y.Y., Gao, W., Shahpar, Z., Emaminejad, S., Challa, S., Chen, K., Fahad, H.M., Tai, L.-C., Ota, H., Davis, R.W., 2016. ACS Nano 10(7), 7216-7224.
Pabari, R., Ramtoola, Z., 2012. J. Young Pharm. 4(3), 157-163.
Peltola, E., Sainio, S., Holt, K.B., Palomäki, T., Koskinen, J., Laurila, T., 2017. Anal. Chem. 90(2), 1408-1416.
Prasad, A., Sankar, M.R., Katiyar, V., 2017. Mater. Today-Proc. 4(2), 898-907.
Prince, M., Ali, G.-C., Guerchet, M., Prina, A.M., Albanese, E., Wu, Y.-T., 2016. Alzheimers Res. Ther. 8(1), 23.
Ruckh, T.T., Clark, H.A., 2014. Anal. Chem.Anal. Chem. 86(3), 1314-1323.
Suominen, T., Uutela, P., Ketola, R.A., Bergquist, J., Hillered, L., Finel, M., Zhang, H., Laakso, A., Kostiainen, R., 2013. Plos One 8(6), e68007.
Thakur, N., Das Adhikary, S., Kumar, M., Mehta, D., Padhan, A.K., Mandal, D., Nagaiah, T.C., 2018. ACS Omega 3(3), 2966-2973.
Wang, J., Yang, B., Zhong, J., Yan, B., Zhang, K., Zhai, C., Shiraishi, Y., Du, Y., Yang, P., 2017. J. Colloid. Interface Sci. 497, 172-180.
Zhou, J., Sheng, M., Jiang, X., Wu, G., Gao, F., 2013. Sensors 13(10), 14029-14040.
Zuo, P.-P., Feng, H.-F., Xu, Z.-Z., Zhang, L.-F., Zhang, Y.-L., Xia, W., Zhang, W.-Q., 2013. Chem. Cent. J. 7(1), 39.